






Ice nucleation by aerosols from anthropogenic pollution

Bin Zhao ^{1,6*}, Yuan Wang ^{2,3,6*}, Yu Gu ^{1*}, Kuo-Nan Liou¹, Jonathan H. Jiang³, Jiwen Fan ⁴, Xiaohong Liu ⁵, Lei Huang³ and Yuk L. Yung^{2,3}

The formation of ice particles in the atmosphere strongly affects cloud properties and the climate. While mineral dust is known to be an effective ice nucleating particle, the role of aerosols from anthropogenic pollution in ice nucleation is still under debate. Here we probe the ice nucleation ability of different aerosol types by combining 11-year observations from multiple satellites and cloud-resolving model simulations. We find that, for strong convective systems, the ice particle effective radius near cloud top decreases with increasing loading of polluted continental aerosols, because the ice formation is dominated by homogeneous freezing of cloud droplets, which are smaller under more polluted conditions. By contrast, an increase in ice particle effective radius with polluted continental aerosols is found for moderate convection. Our model simulations suggest that this positive correlation is explained by enhanced heterogeneous ice nucleation and prolonged ice particle growth at higher aerosol loading, indicating that polluted continental aerosols contain a considerable fraction of ice nucleating particles. Similar aerosol-ice relationships are observed for dust aerosols, further corroborating the ice nucleation ability of polluted continental aerosols. By catalysing ice formation, aerosols from anthropogenic pollution could have profound impacts on cloud lifetime and radiative effect as well as precipitation efficiency.

The ice formation process determines cloud hydrometeor number and size, alters cloud fraction and lifetime and subsequently affects the radiative balance^{1,2}. Atmospheric ice formation also plays a pivotal role in the global hydrological cycle, since most precipitation initiates through ice-phase processes over land^{3,4}. Ice nucleation occurs following two primary pathways: homogeneous freezing of supercooled cloud droplets or solution particles below about -37°C (ref. ⁵), and heterogeneous nucleation triggered by ice nucleating particles (INPs)^{6,7}. INPs possess surface properties lowering the energy barrier for deposition nucleation or droplet freezing⁷⁻¹⁰. Although representing only 1 out of 10^3 – 10^6 ambient particles at about -10 to -37°C (ref. ⁶), INPs can exert an important influence on cloud microphysical properties, such as ice particle number and size^{2,6}.

Previous studies on ice nucleating properties of aerosols mainly relied on experiments under controlled environmental conditions, using either laboratory-generated or field-collected aerosol samples^{7,11,12}. Additionally, many studies attempted to deduce the ice nucleation ability of different aerosol constituents by examining chemical compositions of ice residuals, which are particles remaining after evaporation of field-collected ice hydrometeors^{13,14}. Mineral dust and biological aerosols are commonly believed to dominate the INP budget^{11,15}, while several aerosol constituents of anthropogenic origin have also been suggested to act as INPs, such as soot^{16,17}, glassy organic aerosols^{7,18-20}, metallic (especially lead-containing) aerosols^{14,21} and solid ammonium sulfate¹². For instance, Knopf et al.¹⁸ indicated the potential contribution of anthropogenic organic particles to cirrus formation from measurements in the highly polluted environment of Mexico City. Cziczo et al.¹⁴ revealed that a dominant component of ice residuals of cirrus clouds was

metallic particles, next to mineral dust. Lacher et al.²² found that injections from polluted continental air masses led to increases in INP concentrations in mixed-phase cloud conditions. However, anthropogenic pollution aerosols are chemically complex and may change over time and vary from region to region (due to photochemical processing, mixing state variations, phase state change, cloud recycling and so on), and thus different studies showed contradictory ice nucleation activities^{7,12,13,16}. To evaluate the overall ice nucleation ability of anthropogenic pollution aerosols over a large spatiotemporal domain, we adopt a top-down approach by assessing the bulk relationships between different types of aerosol and ice particle properties.

A number of space-borne sensors orbiting the Earth produce global continuous measurements of aerosol and cloud properties. However, a major difficulty in assessing ice nucleation activities from space is that these measurements only provide states of clouds resulting from numerous dynamical and microphysical processes (for example, ice multiplication, rimming, coagulation and deposition), not just ice nucleation. Our recent study²³ showed that the response of ice particle effective radius (R_{ei}) of cirrus clouds to aerosol loading could be either negative (Twomey effect) or positive (anti-Twomey effect), depending on meteorological conditions. The meteorological modulation of R_{ei} -aerosol relationships directly results from the competition between homogeneous and heterogeneous ice nucleation, thus providing a new perspective to assess the role of various aerosol types in ice nucleation. In this study, we combine 11-year continuous satellite observations from the A-Train constellation and cloud-resolving simulations to scrutinize ice nucleation initiated by various aerosol types, with a focus on aerosols from anthropogenic pollution. The study region is East

¹Joint Institute for Regional Earth System Science and Engineering and Department of Atmospheric and Oceanic Sciences, University of California, Los Angeles, CA, USA. ²Division of Geological and Planetary Sciences, California Institute of Technology, Pasadena, CA, USA. ³Jet Propulsion Laboratory, California Institute of Technology, Pasadena, CA, USA. ⁴Atmospheric Sciences and Global Change Division, Pacific Northwest National Laboratory, Richland, WA, USA. ⁵Department of Atmospheric Science, University of Wyoming, Laramie, WY, USA. ⁶These authors contributed equally: B. Zhao, Y. Wang. *e-mail: zhaob1206@ucla.edu; yuan.wang@caltech.edu; gu@atmos.ucla.edu

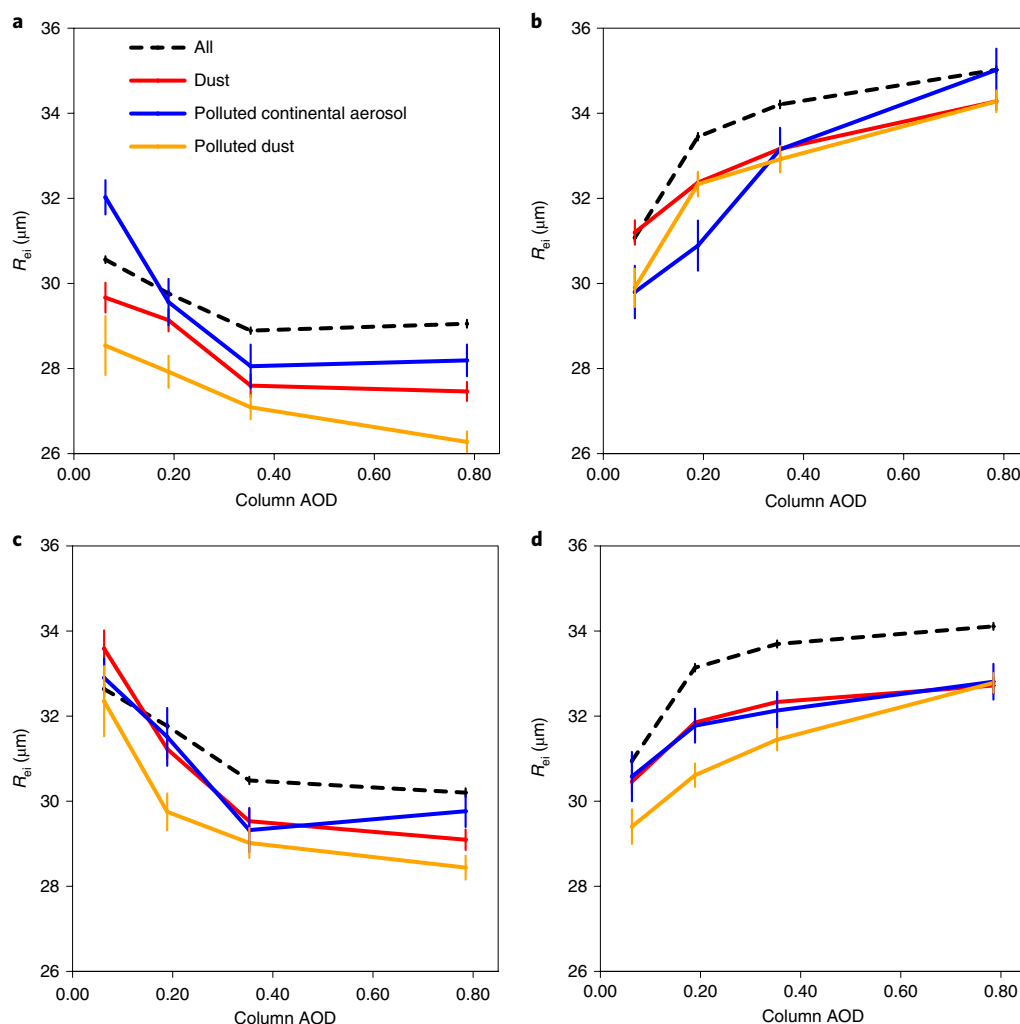


Fig. 1 | Relationships between column AOD and R_{ei} of cold-top convective clouds and anvil cirrus with different ranges of CTH or CAPE. **a, >67% percentile of CTH. **b**, <33% percentile of CTH. **c**, >67% percentile of CAPE. **d**, <33% percentile of CAPE. For each CTH/CAPE group, AOD of each aerosol type is divided into four bins with increasing AOD values. The error bars denote the s.e.m. (σ/\sqrt{N}) of the bin, where σ is the s.d. and N is the sample number.**

Asia (Supplementary Fig. 1), which has a wide range of aerosol type and loading^{24,25}.

Results and discussion

Satellite-derived relationships between aerosol and R_{ei} . We analyse changes in R_{ei} retrieved by MODIS (Moderate Resolution Imaging Spectroradiometer) as a function of aerosol optical depth (AOD), which is a proxy for aerosol loading (Fig. 1). We focus on convective clouds with cloud-top temperature colder than -37°C (cold-top convective clouds hereafter) and anvil cirrus generated from them. Such anvil cirrus was also classified as liquid-origin cirrus by Krämer et al.²⁶ The temperature threshold applied here is to include the influence of homogeneous freezing. Since the retrieval of R_{ei} by MODIS is dominated by ice particles near cloud top²⁷, the R_{ei} used in this study generally corresponds to the ice particles located above the height of the -37°C isotherm. We divide all samples into three equal subsets on the basis of cloud-top height (CTH), which approximately indicates the relative strength of convection²⁸. We show the R_{ei} -AOD relationships separately for the above-67th-percentile group (CTH > 13.1 km, Fig. 1a) and the below-33rd-percentile group (CTH < 11.0 km, Fig. 1b). The R_{ei} decreases significantly with an increase in total AOD (black dashed lines in Fig. 1) for clouds with high CTH, similar to the conventional Twomey effect for liquid

clouds²⁹. By contrast, for clouds with low CTH, R_{ei} increases remarkably with AOD at small-to-moderate AOD range (<~0.4) and levels off at larger AOD. Similarly, we group the samples on the basis of surface-based convective available potential energy (CAPE), which is a measure of the maximal energy available for convection to consume³⁰. We find a good correlation between CAPE and CTH for our samples (coefficient about 0.6). Figure 1c,d shows that the R_{ei} -AOD relationships under high and low CAPE strongly resemble those for high and low CTH, respectively. Therefore, convective strength modulates the observed R_{ei} -AOD relationships.

We employ satellite measurements from CALIOP (Cloud-Aerosol Lidar with Orthogonal Polarization) and AIRS (Atmospheric Infrared Sounder) to classify aerosol types. The R_{ei} -AOD relationships for dust, polluted continental aerosol and polluted dust (coloured solid lines in Fig. 1) are similar to those for the total AOD. There are significant negative and positive correlations with relatively strong convection (implied by high CTH or CAPE) and moderate convection (low CTH or CAPE), respectively, for any of the three aerosol types. Note that polluted continental aerosols in this study do not include soil/anthropogenic dust or smoke, which are classified as separate types, according to the CALIOP and AIRS retrieval algorithms^{31,32}. We further separately analyse cold-top convective clouds and convection-generated anvil cirrus, and find that

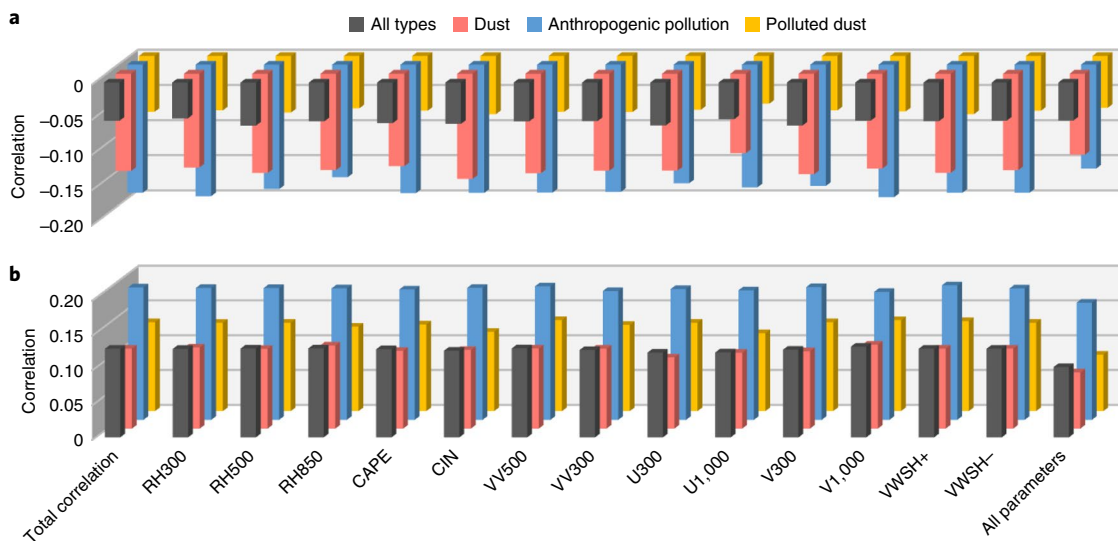


Fig. 2 | Pearson's total and partial correlations between AOD and R_{ice} . **a**, >67% percentile of CTH. **b**, <33% percentile of CTH. The leftmost column represents the total correlation, and the other columns represent partial correlations with effects of 13 meteorological parameters all eliminated simultaneously (rightmost column) and individually (all other columns). The magnitude of the correlation is not large, since R_{ice} is affected by many factors other than aerosols. However, all correlations in this figure are statistically significant at the 0.01 level on the basis of the Student *t*-test. The AOD range is [0, 0.8]. The meanings of the meteorological parameters are provided in Methods.

the opposite R_{ice} –AOD relationships are present for both cloud types (Supplementary Fig. 2). For warm-top convective clouds (cloud-top temperature > -30°C), however, R_{ice} is insensitive to the AOD of any aerosol type (Supplementary Fig. 3). Here we hypothesize that the aerosol effect on R_{ice} depends on the relative importance of heterogeneous and homogeneous ice nucleation, which is further subject to the convective strength. To test this hypothesis and understand the underlying physical mechanisms, we perform model simulations with different perturbations of cloud condensation nuclei (CCNs) and INPs (see the next section).

One possible cause of the observed R_{ice} –AOD relationships is the covariations of meteorological conditions that lead to simultaneous changes in R_{ice} and AOD. Here we use a partial correlation analysis to examine such a possibility. The partial correlation is a measure of the dependence between two variables (R_{ice} and AOD) when the influence of possible controlling variables (meteorological parameters) is removed^{33,34}. Figure 2 and Supplementary Fig. 4 summarize the total correlations as well as the partial correlations with the effects of 13 meteorological parameters eliminated individually and simultaneously. Similarity between the partial and total correlations indicates that the observed R_{ice} –AOD correlations are not significantly attributable to meteorological covariations. For each aerosol type and CTH/CAPE range, we find that the partial correlations eliminating any or all meteorological parameter(s) always have the same sign as the corresponding total correlations, and the relative differences between the two are always within 30%, indicating that the majority ($\geq 70\%$) of the correlations are attributable to the aerosol effect. More details of our statistical method and result interpretation are provided in Supplementary Information.

Cloud-resolving simulations of the aerosol effects. We conduct model simulations using the Weather Research and Forecasting model equipped with a spectral-bin cloud microphysics (WRF-SBM) and aerosol-aware heterogeneous ice nucleation schemes^{35–37} for two cold-top convective cloud systems occurring in our satellite-analysis domain. The two cases were chosen to represent two typical convection systems, one with moderate and one with strong convective strength. For each cloud system, we perform a baseline experiment

with four numerical simulations in which the number concentrations of aerosols (here confined to be hygroscopic particles with diameter greater than $0.1\ \mu\text{m}$ that could serve as CCNs under favourable supersaturation) are 100, 600, 1,600 and $3,200\ \text{cm}^{-3}$, covering clean to polluted conditions^{38–40}. In each simulation, the average INP fraction is estimated to be about $1/20,000$, on the basis of the heterogeneously nucleated ice number concentration predicted dynamically and the total aerosol concentration initialized in our simulations. Thus, the INP number concentration increases proportionally from about 5 to $160\ \text{l}^{-1}$ when CCN increases from 100 to $3,200\ \text{cm}^{-3}$.

Figure 3 summarizes the simulated R_{ice} and fraction of heterogeneously formed ice crystals as a function of aerosol concentration. In a rising air parcel, heterogeneous nucleation occurs ahead of homogeneous freezing because of a lower requirement on temperature/supersaturation. With high convective strength (Fig. 3a,b), an abundant amount of water vapour is transported rapidly to the upper troposphere. In this situation, heterogeneous nucleation consumes only a small portion of available water vapour or droplets, since INPs represent only 1 out of 20,000 ambient particles. As a result, over 90% of the ice crystals are produced by homogeneous freezing of cloud droplets in all simulations (Fig. 3b). An increase in aerosol concentration leads to the formation of more and smaller cloud droplets (the Twomey effect²⁹), and hence more and smaller ice crystals. In other words, R_{ice} decreases with an increase in aerosol loading (Fig. 3a), consistent with the observations (Fig. 1a,c). Under moderate convective conditions (Fig. 3c,d), however, a limited amount of water vapour is available for cloud formation in the upper troposphere. The heterogeneous nucleation and subsequent ice crystal growth can efficiently compete with and even prevent homogeneous freezing, as indicated by the fact that the fraction of heterogeneously formed ice particles increases from less than 10% to 50% with an increase in INPs from clean to pollution conditions (red line in Fig. 3d). Since the outburst of homogeneous freezing could produce a much larger number of ice particles than its heterogeneous counterpart, an increase in INP concentration (along with an increase in aerosol concentration) would result in a net decrease in ice particle number concentration and thus an increase in R_{ice} (red line in Fig. 3c), also consistent with the observations

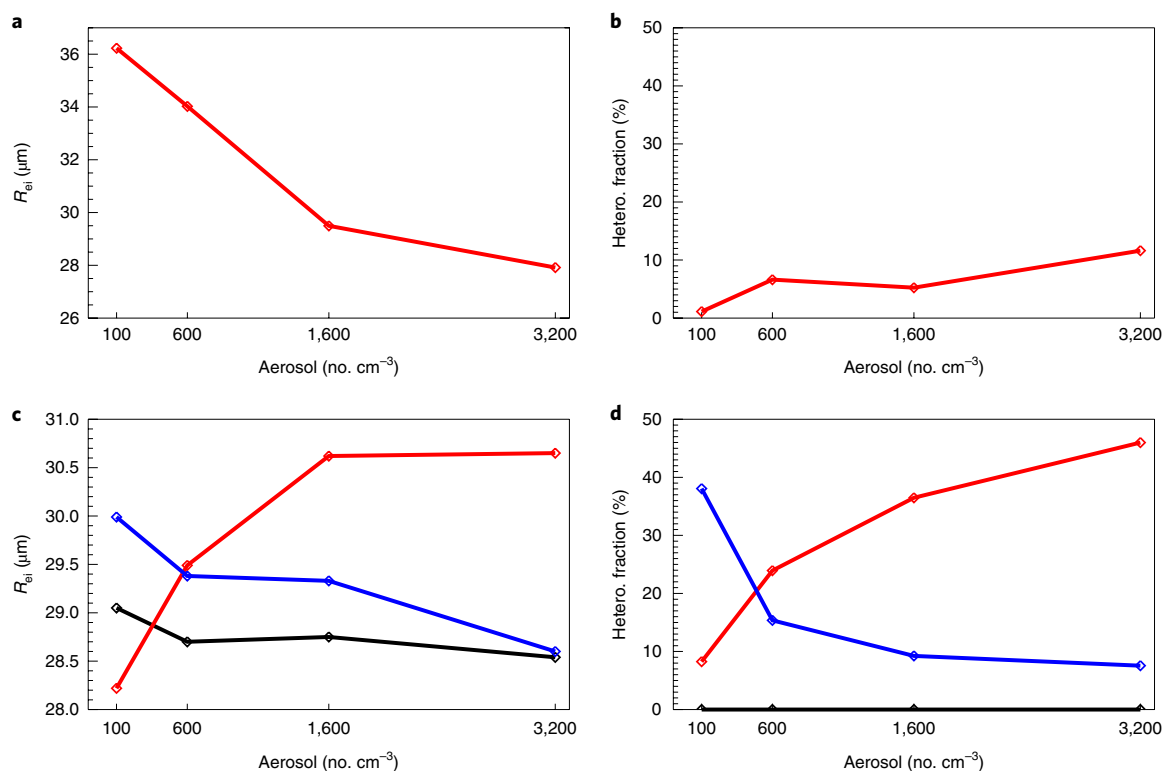


Fig. 3 | Simulated changes in R_{ei} and fraction of heterogeneously formed ice particle number concentration for aerosols with diameter larger than $0.1\ \mu\text{m}$. **a,b**, Strong convection system. **c,d**, Moderate convection system. **a,c**, R_{ei} . **b,d**, Fraction of heterogeneously formed ice particle number concentration. In the baseline simulations (red lines), the number concentrations of INPs increase proportionally with total aerosols. Black and blue lines indicate the results from two groups of sensitivity simulations in which the INP concentrations are fixed at a minimal level ($0.02\ \text{l}^{-1}$) and at $20\ \text{l}^{-1}$, respectively. The R_{ei} are averaged over the grid points colder than $-37\ ^\circ\text{C}$.

(Fig. 1b, d). This phenomenon, known as the anti-Twomey effect, has been found in previous studies^{41,42}. The convective-strength modulation works not only by changing upper tropospheric water vapour amount, but also by altering updraught velocity. A stronger convection is typically characterized as higher updraught velocity, which is favourable for homogeneous freezing by reducing the growth time of heterogeneously formed ice crystals. The above mechanism also explains the insensitive response of R_{ei} to AOD for warm-top convective clouds (cloud-top temperature $> -30\ ^\circ\text{C}$, Supplementary Fig. 3). In these cases, an excessive amount of water vapour is available for ice crystal growth, because homogeneous freezing is not triggered and only limited ice particles are generated from heterogeneous nucleation.

To further demonstrate that INPs play a key role in reproducing the observed R_{ei} -aerosol relationships, we perform additional two groups of sensitivity simulations in which the INP concentrations are fixed at a minimal level ($0.02\ \text{l}^{-1}$) and at $20\ \text{l}^{-1}$ for the moderate convection system (black and blue lines in Fig. 3c,d). In both groups, the concentrations of aerosol with diameter larger than $0.1\ \mu\text{m}$ vary in the same range as the baseline simulations, that is, $100\text{--}3,200\ \text{cm}^{-3}$. It turns out that R_{ei} decreases slightly with aerosol concentration in both groups of sensitivity simulations (black and blue lines in Fig. 3c), in contrast to the observed positive correlation between R_{ei} and aerosol loading (Fig. 1b,d). This means that the observed R_{ei} -aerosol relationships (Fig. 1) would not occur if INPs were not present, or if INPs did not change with the total aerosol concentrations.

Anthropogenic pollution aerosols as INPs. For polluted continental aerosols, the satellite data show opposite R_{ei} -AOD relationships

for strong and for moderate convection (Fig. 1). Meanwhile, cloud-resolving sensitivity simulations demonstrate that the opposite R_{ei} -aerosol relationships under different convective strengths can be produced only if INP concentration is roughly proportional to total aerosol concentration. Therefore, we conclude that a portion of polluted continental aerosols can serve as INPs. If INPs were absent or remained invariant along with increases in polluted continental aerosols, the observed positive correlation between R_{ei} and polluted continental AOD under moderate convection would be reversed, as illustrated by the comparison of different groups of model simulations (Fig. 3c). Moreover, the similar observed R_{ei} -AOD relationships between dust (well defined INPs) and polluted continental aerosols corroborate that a portion of polluted continental aerosols possess a certain ice nucleating ability. The effects of aerosols from anthropogenic pollution, serving as both INPs and CCNs, on microphysical properties of cold-top convective clouds are summarized in Fig. 4.

We note that the robustness of our conclusion for anthropogenic pollution aerosols acting as INPs is subject to the uncertainty in satellite-derived aerosol type. To minimize this uncertainty, we only select samples with the same aerosol type within a 50-km radius and further filter dust out of polluted continental samples using independent retrievals from AIRS. Also note that anthropogenic pollution is more severe in stagnant conditions and urban areas, while dust concentration is usually higher in windy conditions and biological aerosol is more prevalent in remote areas^{43,44}. Even if dust or biological aerosols (both being well defined INPs^{11,12}) exist in some polluted continental samples occasionally, concentrations of these contaminants are unlikely to increase proportionally with those of polluted continental aerosols and thus still cannot explain the

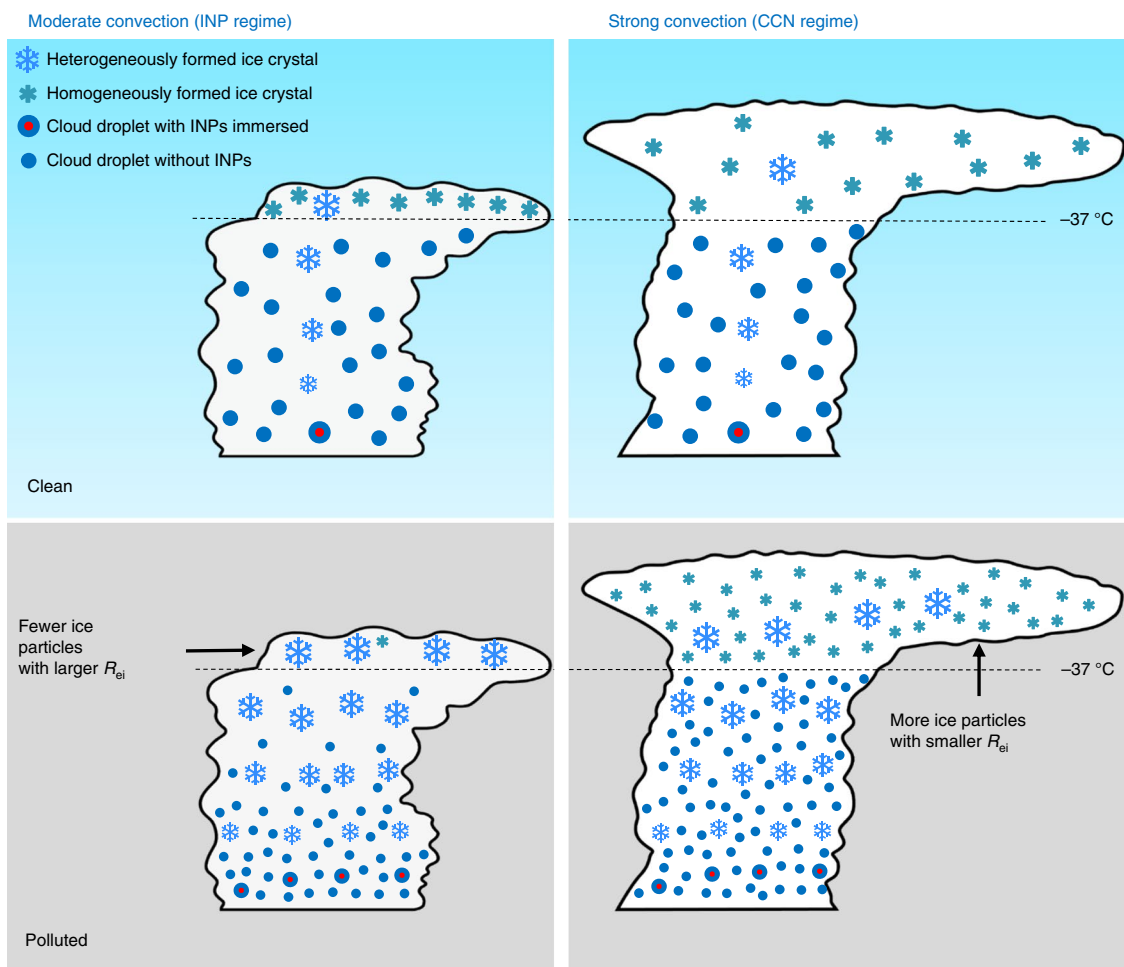


Fig. 4 | Schematic of microphysical changes in cold-top convective clouds due to an increase in loading of anthropogenic pollution aerosols. Under strong convection, ice crystals above the $-37\text{ }^{\circ}\text{C}$ isotherm are primarily produced by homogeneous freezing. An increase in aerosol loading leads to the formation of more and smaller ice crystals. Under moderate convection, with an increase in INPs from clean to polluted conditions, heterogeneous nucleation gradually overtakes homogeneous freezing, resulting in a decrease in ice particle number concentration and thus an increase in R_{ri} . Aerosol-induced changes in cloud macrophysics and dynamics, such as the aerosol invigoration effect^{49,50}, are not illustrated.

observed R_{ri} –aerosol relationships. In summary, our conclusion is not prone to the imperfection of aerosol typing in satellite retrievals.

In the present study we demonstrate that aerosols from anthropogenic pollution contain a considerable fraction of INPs using a top-down approach. The results thus provide a valuable constraint on estimates of the anthropogenic INP budget in modelling studies. An unresolved question in this study is what constituent contributes a major fraction of the INPs from anthropogenic pollution. The potential candidates are discussed in Supplementary Information. In the future, we expect more bottom-up model simulations of INPs from individual anthropogenic aerosol species, and comparison of these simulations with our top-down analysis results. Furthermore, our finding has important implications for global and regional climate studies. By acting as INPs, anthropogenic aerosols could have profound impacts on cloud lifetime and radiative effect as well as precipitation efficiency^{2,6,45}. To date, only a few studies have considered the heterogeneous ice nucleation by certain aerosol species from anthropogenic pollution in climate models^{45–47}. Incorporation of this process may change cloud glaciation rate⁴⁸ and hence result in a different anthropogenic radiative forcing from preindustrial times to the present day. It also benefits the assessment of changes in the Earth's hydrology cycle and the distribution of water resources.

Online content

Any methods, additional references, Nature Research reporting summaries, source data, statements of code and data availability and associated accession codes are available at <https://doi.org/10.1038/s41561-019-0389-4>.

Received: 16 December 2018; Accepted: 15 May 2019;
Published online: 1 July 2019

References

1. IPCC *Climate Change 2013: The Physical Science Basis* (eds Stocker, T. F. et al.) (Cambridge Univ. Press, 2013).
2. Seinfeld, J. H. et al. Improving our fundamental understanding of the role of aerosol–cloud interactions in the climate system. *Proc. Natl Acad. Sci. USA* **113**, 5781–5790 (2016).
3. Mühlmenstädt, J., Sourdeval, O., Delanoë, J. & Quaas, J. Frequency of occurrence of rain from liquid-, mixed-, and ice-phase clouds derived from A-Train satellite retrievals. *Geophys. Res. Lett.* **42**, 6502–6509 (2015).
4. Wang, Y. et al. Long-term impacts of aerosols on precipitation and lightning over the Pearl River Delta megacity area in China. *Atmos. Chem. Phys.* **11**, 12421–12436 (2011).
5. Koop, T., Luo, B. P., Tsias, A. & Peter, T. Water activity as the determinant for homogeneous ice nucleation in aqueous solutions. *Nature* **406**, 611–614 (2000).
6. DeMott, P. J. et al. Predicting global atmospheric ice nuclei distributions and their impacts on climate. *Proc. Natl Acad. Sci. USA* **107**, 11217–11222 (2010).

7. Knopf, D. A., Alpert, P. A. & Wang, B. B. The role of organic aerosol in atmospheric ice nucleation: a review. *ACS Earth Space Chem.* **2**, 168–202 (2018).
8. Kiselev, A. et al. Active sites in heterogeneous ice nucleation—the example of K-rich feldspars. *Science* **355**, 367–371 (2017).
9. Bi, Y. F., Cao, B. X. & Li, T. S. Enhanced heterogeneous ice nucleation by special surface geometry. *Nat. Commun.* **8**, 15372 (2017).
10. Holden, M. A. et al. High-speed imaging of ice nucleation in water proves the existence of active sites. *Sci. Adv.* **5**, eaav4316 (2019).
11. Hoose, C. & Moehler, O. Heterogeneous ice nucleation on atmospheric aerosols: a review of results from laboratory experiments. *Atmos. Chem. Phys.* **12**, 9817–9854 (2012).
12. Kanji, Z. A. et al. in *Ice Formation and Evolution in Clouds and Precipitation: Measurement and Modeling Challenges* (eds Baumgardner, D., McFarquhar, G. M. & Heymsfield, A. J.) Vol. 58, 1.1–1.33 (American Meteorological Society, 2017).
13. Cziczo, D. J. et al. in *Ice Formation and Evolution in Clouds and Precipitation: Measurement and Modeling Challenges* (eds Baumgardner, D., McFarquhar, G. M. & Heymsfield, A. J.) Vol. 58, 8.1–8.13 (American Meteorological Society, 2017).
14. Cziczo, D. J. et al. Clarifying the dominant sources and mechanisms of cirrus cloud formation. *Science* **340**, 1320–1324 (2013).
15. Murray, B. J., O'Sullivan, D., Atkinson, J. D. & Webb, M. E. Ice nucleation by particles immersed in supercooled cloud droplets. *Chem. Soc. Rev.* **41**, 6519–6554 (2012).
16. Bond, T. C. et al. Bounding the role of black carbon in the climate system: a scientific assessment. *J. Geophys. Res. Atmos.* **118**, 5380–5552 (2013).
17. Mahrt, F. et al. Ice nucleation abilities of soot particles determined with the Horizontal Ice Nucleation Chamber. *Atmos. Chem. Phys.* **18**, 13363–13392 (2018).
18. Knopf, D. A., Wang, B., Laskin, A., Moffet, R. C. & Gilles, M. K. Heterogeneous nucleation of ice on anthropogenic organic particles collected in Mexico City. *Geophys. Res. Lett.* **37**, L11803 (2010).
19. Wang, B. et al. Heterogeneous ice nucleation and water uptake by field-collected atmospheric particles below 273 K. *J. Geophys. Res. Atmos.* **117**, D00v19 (2012).
20. China, S. et al. Ice cloud formation potential by free tropospheric particles from long-range transport over the Northern Atlantic Ocean. *J. Geophys. Res. Atmos.* **122**, 3065–3079 (2017).
21. Cziczo, D. J. et al. Inadvertent climate modification due to anthropogenic lead. *Nat. Geosci.* **2**, 333–336 (2009).
22. Lacher, L. et al. Impact of air mass conditions and aerosol properties on ice nucleating particle concentrations at the High Altitude Research Station Jungfraujoch. *Atmosphere* **9**, 363 (2018).
23. Zhao, B. et al. Impact of aerosols on ice crystal size. *Atmos. Chem. Phys.* **18**, 1065–1078 (2018).
24. Wang, J. D. et al. Particulate matter pollution over China and the effects of control policies. *Sci. Total Environ.* **584**, 426–447 (2017).
25. Zhao, B. et al. Intra-annual variations of regional aerosol optical depth, vertical distribution, and particle types from multiple satellite and ground-based observational datasets. *Atmos. Chem. Phys.* **18**, 11247–11260 (2018).
26. Krämer, M. et al. A microphysics guide to cirrus clouds—Part 1: Cirrus types. *Atmos. Chem. Phys.* **16**, 3463–3483 (2016).
27. Stein, T. H. M., Delanoë, J. & Hogan, R. J. A comparison among four different retrieval methods for ice-cloud properties using data from CloudSat, CALIPSO, and MODIS. *J. Appl. Meteorol. Climatol.* **50**, 1952–1969 (2011).
28. Sherwood, S. C., Minnis, P. & McGill, M. Deep convective cloud-top heights and their thermodynamic control during CRYSTAL-FACE. *J. Geophys. Res. Atmos.* **109**, D20119 (2004).
29. Twomey, S. Influence of pollution on shortwave albedo of clouds. *J. Atmos. Sci.* **34**, 1149–1152 (1977).
30. Gartzke, J., Knuteson, R., Przybyl, G., Ackerman, S. & Revercomb, H. Comparison of satellite-, model-, and radiosonde-derived convective available potential energy in the Southern Great Plains region. *J. Appl. Meteorol. Climatol.* **56**, 1499–1513 (2017).
31. Omar, A. H. et al. The CALIPSO automated aerosol classification and lidar ratio selection algorithm. *J. Atmos. Ocean. Technol.* **26**, 1994–2014 (2009).
32. DeSouza-Machado, S. G. et al. Infrared retrievals of dust using AIRS: comparisons of optical depths and heights derived for a North African dust storm to other collocated EOS A-Train and surface observations. *J. Geophys. Res. Atmos.* **115**, D15201 (2010).
33. Hardle, W. K. & Simar, L. *Applied Multivariate Statistical Analysis* 4th edn, 773 (Springer, 2015).
34. Zhao, B. et al. Type-dependent responses of ice cloud properties to aerosols from satellite retrievals. *Geophys. Res. Lett.* **45**, 3297–3306 (2018).
35. Fan, J. et al. Aerosol impacts on California winter clouds and precipitation during CalWater 2011: local pollution versus long-range transported dust. *Atmos. Chem. Phys.* **14**, 81–101 (2014).
36. Fan, J. W., Leung, L. R., Rosenfeld, D. & DeMott, P. J. Effects of cloud condensation nuclei and ice nucleating particles on precipitation processes and supercooled liquid in mixed-phase orographic clouds. *Atmos. Chem. Phys.* **17**, 1017–1035 (2017).
37. Wang, Y., Fan, J. W., Zhang, R. Y., Leung, L. R. & Franklin, C. Improving bulk microphysics parameterizations in simulations of aerosol effects. *J. Geophys. Res. Atmos.* **118**, 5361–5379 (2013).
38. Schmale, J. et al. Long-term cloud condensation nuclei number concentration, particle number size distribution and chemical composition measurements at regionally representative observatories. *Atmos. Chem. Phys.* **18**, 2853–2881 (2018).
39. Yang, J. F., Lei, H. C. & Lu, Y. H. Airborne observations of cloud condensation nuclei spectra and aerosols over East Inner Mongolia. *Adv. Atmos. Sci.* **34**, 1003–1016 (2017).
40. Cai, M. et al. The size resolved cloud condensation nuclei (CCN) activity and its prediction based on aerosol hygroscopicity and composition in the Pearl Delta River (PRD) Region during wintertime 2014. *Atmos. Chem. Phys.* **18**, 16419–16437 (2018).
41. Kärcher, B. & Lohmann, U. A parameterization of cirrus cloud formation: heterogeneous freezing. *J. Geophys. Res. Atmos.* **108**, 4402 (2003).
42. Spichtinger, P. & Cziczo, D. J. Impact of heterogeneous ice nuclei on homogeneous freezing events in cirrus clouds. *J. Geophys. Res. Atmos.* **115**, D14208 (2010).
43. Shao, Y., Ishizuka, M., Mikami, M. & Leys, J. F. Parameterization of size-resolved dust emission and validation with measurements. *J. Geophys. Res. Atmos.* **116**, D08203 (2011).
44. Despres, V. R. et al. Primary biological aerosol particles in the atmosphere: a review. *Tellus B* **64**, 15598 (2012).
45. Lohmann, U. A glaciation indirect aerosol effect caused by soot aerosols. *Geophys. Res. Lett.* **29**, 1052 (2002).
46. Phillips, V. T. J. et al. Improvements to an empirical parameterization of heterogeneous ice nucleation and its comparison with observations. *J. Atmos. Sci.* **70**, 378–409 (2013).
47. Penner, J. E., Zhou, C., Garnier, A. & Mitchell, D. L. Anthropogenic aerosol indirect effects in cirrus clouds. *J. Geophys. Res. Atmos.* **123**, 11652–11677 (2018).
48. Charnawskas, J. C. et al. Condensed-phase biogenic-anthropogenic interactions with implications for cold cloud formation. *Faraday Discuss.* **200**, 165–194 (2017).
49. Rosenfeld, D. et al. Flood or drought: how do aerosols affect precipitation? *Science* **321**, 1309–1313 (2008).
50. Fan, J. W. et al. Substantial convection and precipitation enhancements by ultrafine aerosol particles. *Science* **359**, 411–418 (2018).

Acknowledgements

This study is supported by the NASA ROSES TANPP (80NSSC18K0985) and NSF AGS-1701526, AGS-1700727 and AGS-1642289 grants. We acknowledge the support of the Jet Propulsion Laboratory, California Institute of Technology, under contract with NASA, and the Joint Institute for Regional Earth System Science and Engineering at the University of California Los Angeles. The effort of J.F. was supported by the US Department of Energy (DOE) Early Career Research Program. X.L. was supported by the US DOE Atmospheric System Research Program (grants DE-SC0014239 and DE-SC0018926). We would like to acknowledge high-performance computing support from Cheyenne (<https://doi.org/10.5065/D6RX99HX>) provided by NCAR's Computational and Information Systems Laboratory, sponsored by the National Science Foundation.

Author contributions

B.Z., Y.G. and Y.W. designed the research; B.Z., Y.G., Y.W. and L.H. performed the satellite data analysis; Y.W., B.Z. and J.F. performed the model simulation; B.Z., Y.W., Y.G., K.-N.L., J.F., J.H.J. and X.L. analysed the results; B.Z., Y.W., Y.G., K.-N.L., J.H.J., J.F., X.L. and Y.L.Y. wrote the paper.

Competing interests

The authors declare no competing interests.

Additional information

Supplementary information is available for this paper at <https://doi.org/10.1038/s41561-019-0389-4>.

Reprints and permissions information is available at www.nature.com/reprints.

Correspondence and requests for materials should be addressed to B.Z., Y.W. or Y.G.

Publisher's note: Springer Nature remains neutral with regard to jurisdictional claims in published maps and institutional affiliations.

© The Author(s), under exclusive licence to Springer Nature Limited 2019

Methods

Sources and processing of satellite retrievals. We use collocated observations of aerosol and cloud properties from CALIOP aboard CALIPSO (Cloud–Aerosol Lidar and Infrared Pathfinder Satellite Observations), and MODIS and AIRS aboard Aqua, as summarized in Supplementary Table 1.

In this study, we are interested in cold-top convective clouds and anvil cirrus clouds generated from them. We select single-layer clouds of these two types with valid quality assurance flags, on the basis of the CALIOP level 2 merged aerosol and cloud layer product (05kmMLay, V4.10) at a 5 km along-track resolution. The cloud type flag in the CALIOP 05kmMLay product differentiates seven cloud types, among which are deep convective cloud and cirrus. We define a cloud profile as cold-top convective cloud if the cloud type flag is deep convective cloud and the cloud-top temperature is colder than -37°C . The deep convective clouds identified by CALIOP are high and optically thick clouds, which are presumably associated with convection³¹. It is noted that, due to the limited ability of CALIOP to penetrate clouds, these clouds may not necessarily develop from near the surface, which has been used as a criterion for deep convective clouds in some other cloud typing algorithms³². The selection criteria of cold-top convective clouds should not affect the conclusion of this study, because the convective-strength modulation of R_{ci} –aerosol relationships theoretically holds as long as the competition between homogeneous and heterogeneous nucleation takes place. Similarly, the warm-top convective clouds used in the analysis of Supplementary Fig. 3 are selected when the cloud type flag is deep convective cloud and the cloud-top temperature is warmer than -30°C . We use a temperature threshold of more than -30°C to minimize the impact of settlement of homogeneously formed ice particles at heights above the -37°C isotherm.

The cirrus clouds identified by CALIOP include two major types with distinct formation mechanisms: convection generated (anvil) and in situ formed. Following Zhao et al.²³, a cirrus cloud profile is classified as convection generated if it is physically connected to deep convection profiles. Two neighbouring CALIOP cloud layers are considered to be connected if they vertically overlap and are horizontally separated by no more than one profile (that is, distance ≤ 5 km). Zhao et al.²³ also examined the physical properties of convection-generated and in situ-formed cirrus and demonstrated the cirrus type classification to be reasonable.

Subsequently, we match retrievals from other sensors to the CALIOP 5 km profiles, and calculate a number of aerosol/cloud properties corresponding to each cloud profile. The R_{ci} is calculated by averaging the 1×1 km MODIS R_{ci} retrievals (MYD06 product, Collection 6) for which the cloud phase is ice and the R_{ci} uncertainty is smaller than 100%, within a 10-km radius of a CALIOP profile. We only include in the R_{ci} calculation the MODIS pixels that vertically overlap with the CALIOP cloud layer (layer-top pressure of CALIOP cloud layer -10 hPa \leq cloud-top pressure of MODIS ice pixel \leq layer base pressure of CALIOP cloud layer), with the purpose of minimizing contamination by MODIS cloud pixels that do not belong to the same cloud layer as detected by CALIOP.

For a given aerosol type/composition, AOD is roughly proportional to aerosol loading^{33–36}. Therefore, we use AOD as a proxy for a loading of aerosols interacting with convective clouds and convection-generated anvil cirrus, which has been a common practice in previous satellite-based studies on aerosol–cloud interactions^{23,37–42}. We use the column-integrated AOD because convective clouds are developed from the lower troposphere and thus can be affected by aerosols at various altitudes. Using aerosol information from specific layers may not fully capture all aerosol effects discussed in this study. Similarly to R_{ci} , AOD is estimated using the mean of all 10×10 km² MODIS AOD retrievals (MYD04 product, Collection 6) within a 50-km radius of a CALIOP profile. As AOD retrievals by MODIS are usually missing at cloudy scenes, we do the averaging over a relatively large area to increase the number of samples with valid AOD values, following many previous studies^{57,58,62}. The spatially averaged AOD should be representative of the CALIOP cloud profile considering the large spatial length scale of 40–400 km for AOD variation.

We classify the selected profiles into various aerosol types primarily on the basis of the CALIOP 05kmMLay product, and further refine the classification using the AIRS level 1B infrared radiance products (AIRBRAD). The aerosol types distinguished by CALIOP include dust, polluted dust, clean continental, polluted continental, smoke, clean marine and dusty marine⁶³. For each CALIOP cloud profile, if all aerosol layers in all profiles within a 50-km radius possess the same aerosol type, it is defined as an aerosol environment of that particular type. This stringent selection criterion is expected to minimize the possibility that different aerosol types are mixed in the retrievals. To ensure that the environment of polluted continental aerosols is not contaminated by dust, we eliminate a polluted continental cloud profile from analysis if ‘dust_score’ from the AIRS AIRBRAD product (which is based on infrared absorption) is larger than or equal to 380 (indicating that dust probably exists⁶⁴) at any location within a 50-km radius of that cloud profile. Fewer than 1% of all profiles with polluted continental aerosols have been removed.

Finally, to evaluate the impact of meteorology on observed aerosol–cloud relationships, we obtain a series of meteorological parameters (Supplementary Table 1) from the CALIOP 05kmAPro product (V4.10) and the Final Analysis reanalysis data product of National Centers for Environmental Prediction (NCEP) with $1^{\circ} \times 1^{\circ}$ and 6-h resolutions. We match the NCEP reanalysis data at 6:00 UTC,

which is closest to the satellite overpassing time (5:00 to 8:00 UTC), to CALIOP cloud profiles by determining which NCEP $1^{\circ} \times 1^{\circ}$ grid contains a CALIOP profile. The meteorological parameters used in this study include relative humidity at 300 hPa (RH300), relative humidity at 500 hPa (RH500), relative humidity at 850 hPa (RH850), CAPE, convective inhibition (CIN), pressure vertical velocity at 500 hPa (VV500), pressure vertical velocity at 300 hPa (VV300), U component of wind speed at 300 hPa (U300), U component of wind speed at 1,000 hPa (U1,000), V component of wind speed at 300 hPa (V300), V component of wind speed at 1,000 hPa (V1,000), vertical wind shear at the potential vorticity surface of $2 \times 10^{-6} \text{ K m}^2 \text{ kg}^{-1} \text{ s}^{-1}$ (VWSH+) and vertical wind shear at the potential vorticity surface of $-2 \times 10^{-6} \text{ K m}^2 \text{ kg}^{-1} \text{ s}^{-1}$ (VWSH–). We use CAPE to indicate the maximal energy for convection to consume^{30,65,66}. Although mid-latitude strong convection is not necessarily characterized by high CAPE, the large-scale instability indicated by high CAPE favours the convection development at 13:30 local time when the satellites overpass. Convective inhibition is typically lower than 30 J kg^{-1} for the samples used in the current study, so it is not considered in the classification of samples in Fig. 1.

Cloud-resolving simulations. In this study, we conduct cloud-resolving simulations to confirm our hypothesis that the number of INPs is the key to reproducing the satellite-derived R_{ci} –aerosol relationships under different convection strengths, and to illustrate the underlying mechanisms. We employ the WRF model version 3.6 with a fast SBM cloud microphysics. The simulation domain covers a 300×300 km² area with a 3 km grid resolution. The fast version of SBM incorporated in the WRF model^{35–37} retains the advantages of the full SBM (ref. 67) and produces cloud microphysical and dynamical structure as well as precipitation similar to those of the full SBM (ref. 68). SBM uses four size distribution spectra to represent CCNs as well as three hydrometeors including water drops (cloud and rain), low-density ice (ice and snow) and high-density ice (graupel and hail). Each spectrum is composed of 33 mass bins and the relationship between adjacent bins is determined by the function $m_k = 2m_{k-1}$ (m_k is the mass of a particle in the k th bin). We use the Bigg scheme⁶⁹ to simulate droplet homogeneous freezing at temperatures below -37°C . The homogeneous ice nucleation of solution particles is treated by the Liu and Penner scheme⁷⁰.

Heterogeneous ice crystal formation in our model is linked to ice-friendly aerosol (IFA) through an ice nucleation parameterization. The number concentration of IFA is a prognostic variable in the model. The INP concentration is calculated dynamically as a function of IFA ($n_{\text{IFA},0.5 \mu\text{m}}$) and temperature (T_k), following the parameterization scheme D2015 of DeMott et al.⁷¹:

$$n_{\text{INP}}(T_k) = (\text{cf})(n_{\text{IFA},0.5 \mu\text{m}})^{(\alpha(273.16 - T_k) + \beta)} \exp(\gamma(273.16 - T_k) + \delta)$$

where cf, α , β , γ and δ are constants in our model. The temperature influence on the INP is explicitly considered in our model simulations. We estimate the INP fraction by calculating the ratio of simulated heterogeneously nucleated ice number concentration to the total aerosol concentration initialized in our simulations.

In accordance with the objective of our simulations described above, we focus on the general nucleating ability of aerosols (serving as either CCNs or INPs) in the WRF sensitivity simulations, but not explicitly considering specific aerosol type or chemical composition. Hence, the simulated R_{ci} –aerosol relationships are independent of specific aerosol type/composition. D2015 is an updated version of ref. 6, and includes both the laboratory data from the Aerosol Interactions and Dynamics of the Atmosphere chamber and field campaign data. They have similar formulae, which are functions of number of aerosol particles larger than $0.5 \mu\text{m}$ and ambient air temperature. Since our model does not explicitly consider aerosol chemical compositions, there is no fundamental difference using these two schemes, except that the updated formula has a more efficient ice nucleation rate, which realistically simulated a dust case in a recent study³⁵.

We simulate two cold-top convective cloud systems in real-case settings. The two systems, which occurred on 22 March 2015 and 29 March 2009, are representative of moderate and strong convection, respectively. Supplementary Figure 7 shows the vertical profiles of updraught velocity, specific humidity and temperature in the simulations of the two types of convection. The maximal updraught velocity is much larger in the strong-convection case than in the moderate-convection case. Note that we use AOD in satellite data analysis and concentrations of aerosols with diameter greater than $0.1 \mu\text{m}$ in modelling to represent loading of aerosols interacting with clouds. Since these two variables are both linked to the total aerosol loading, the observed and modelled R_{ci} –aerosol relationships can be compared in this study.

Data availability

The satellite and meteorology data products used in this study are publicly available at the following sites:

MODIS/Aqua MYD04 and MYD06 products: https://earthdata.nasa.gov/CALIOP/CALIPSO_05kmMLay and 05kmAPro products: <https://eosweb.larc.nasa.gov/>
AIRS/Aqua AIRBRAD product: <https://disc.gsfc.nasa.gov/>
NCEP Final Analysis product: <https://rda.ucar.edu/datasets/ds083.2/>

Other data supporting the findings of this study are available within the Article and Supplementary Information.

Code availability

The code of the WRF-SBM model is available at http://www2.mmm.ucar.edu/wrf/users/download/get_source.html. The scripts used to process the satellite data can be requested from the corresponding authors.

References

51. Liu, Z., Omar, A. H., Hu, Y., Vaughan, M. A. & Winker, D. M. *CALIPSO Algorithm Theoretical Basis Document Part 3: Scene Classification Algorithms* (National Aeronautics and Space Administration, 2005); https://www-calipso.larc.nasa.gov/resources/pdfs/PC-SCI-202_Part3_v1.0.pdf
52. Stein, T. H. M., Holloway, C. E., Tobin, I. & Bony, S. Observed relationships between cloud vertical structure and convective aggregation over tropical ocean. *J. Climate* **30**, 2187–2207 (2017).
53. Chin, M. et al. Light absorption by pollution, dust, and biomass burning aerosols: a global model study and evaluation with AERONET measurements. *Ann. Geophys.* **27**, 3439–3464 (2009).
54. Han, Y. et al. Impacts of elevated-aerosol-layer and aerosol type on the correlation of AOD and particulate matter with ground-based and satellite measurements in Nanjing, southeast China. *Sci. Total Environ.* **532**, 195–207 (2015).
55. Kumar, N., Chu, A. & Foster, A. An empirical relationship between PM_{2.5} and aerosol optical depth in Delhi Metropolitan. *Atmos. Environ.* **41**, 4492–4503 (2007).
56. Ginoux, P. et al. Evaluation of aerosol distribution and optical depth in the Geophysical Fluid Dynamics Laboratory coupled model CM2.1 for present climate. *J. Geophys. Res. Atmos.* **111**, D22210 (2006).
57. Niu, F. & Li, Z. Q. Systematic variations of cloud top temperature and precipitation rate with aerosols over the global tropics. *Atmos. Chem. Phys.* **12**, 8491–8498 (2012).
58. Koren, I., Feingold, G. & Remer, L. A. The invigoration of deep convective clouds over the Atlantic: aerosol effect, meteorology or retrieval artifact? *Atmos. Chem. Phys.* **10**, 8855–8872 (2010).
59. Koren, I., Remer, L. A., Altaratz, O., Martins, J. V. & Davidi, A. Aerosol-induced changes of convective cloud anvils produce strong climate warming. *Atmos. Chem. Phys.* **10**, 5001–5010 (2010).
60. Peng, J., Li, Z. Q., Zhang, H., Liu, J. J. & Cribb, M. Systematic changes in cloud radiative forcing with aerosol loading for deep clouds in the tropics. *J. Atmos. Sci.* **73**, 231–249 (2016).
61. Jiang, J. H. et al. Influence of convection and aerosol pollution on ice cloud particle effective radius. *Atmos. Chem. Phys.* **11**, 457–463 (2011).
62. Jiang, J. H. et al. Contrasting effects on deep convective clouds by different types of aerosols. *Nat. Commun.* **9**, 3874 (2018).
63. Kim, M. H. et al. The CALIPSO version 4 automated aerosol classification and lidar ratio selection algorithm. *Atmos. Meas. Tech.* **11**, 6107–6135 (2018).
64. Won, Y.-I. *README Document for AIRS Level-1B Version 5 IR Calibrated Radiance Products: AIRIBRAD, AIRIBRAD_NRT, AIRIBQAP, AIRIBQAP_NRT* https://docserver.gesdisc.eosdis.nasa.gov/repository/Mission/AIRS/3.3_ScienceDataProductDocumentation/3.3.4_ProductGenerationAlgorithms/README.AIRIBRAD.pdf (2008).
65. Seeley, J. T. & Romps, D. M. Why does tropical convective available potential energy (CAPE) increase with warming? *Geophys. Res. Lett.* **42**, 10429–10437 (2015).
66. Riemann-Campe, K., Fraedrich, K. & Lunkeit, F. Global climatology of Convective Available Potential Energy (CAPE) and Convective Inhibition (CIN) in ERA-40 reanalysis. *Atmos. Res.* **93**, 534–545 (2009).
67. Khain, A., Pokrovsky, A., Pinsky, M., Seifert, A. & Phillips, V. Simulation of effects of atmospheric aerosols on deep turbulent convective clouds using a spectral microphysics mixed-phase cumulus cloud model. Part I: Model description and possible applications. *J. Atmos. Sci.* **61**, 2963–2982 (2004).
68. Khain, A. P. Notes on state-of-the-art investigations of aerosol effects on precipitation: a critical review. *Environ. Res. Lett.* **4**, 015004 (2009).
69. Bigg, E. K. The formation of atmospheric ice crystals by the freezing of droplets. *Q. J. R. Meteorol. Soc.* **79**, 510–519 (1953).
70. Liu, X. H. & Penner, J. E. Ice nucleation parameterization for global models. *Meteorol. Z.* **14**, 499–514 (2005).
71. DeMott, P. J. et al. Integrating laboratory and field data to quantify the immersion freezing ice nucleation activity of mineral dust particles. *Atmos. Chem. Phys.* **15**, 393–409 (2015).